Space-time Trefftz-DG approximation for elasto-acoustics

Hélène Barucq, Henri Calandra, Julien Diaz, Elvira Shishenina

To appear in *Applicable Analysis*
Vol. 00, No. 00, Month 20XX, 1–16

Space-time Trefftz-DG approximation for elasto-acoustics

H. Barucq[a], H. Calandra[b], J. Diaz[a] and E. Shishenina[a,b] *

[a] *Magique-3D, Inria, E2S UPPA, CNRS, Pau, France*; [b] *Total SA, Pau, France*

(*v0.0 released January 2018*)

Discontinuous finite element methods have proven their numerical accuracy and flexibility, but they are still criticized for requiring high number of degrees of freedom for computation. There have been some advances with Hybridizable Discontinuous Galerkin (HDG) approximations but essentially in the time-harmonic regime, because the time integration requires implicit schemes.

Another possibility to explore seems to be Trefftz methods, which distinguish themselves by the choice of basis functions: they are local solutions of initial equation. Thus, in case of time-dependent problems, space-time meshes are required.

Classical Trefftz-type approximation uses the exact solutions of Acoustic System (AS) and Elastodynamic System (ES) taken with different frequencies, in order to obtain better numerical errors. We have computed a polynomial basis using the Taylor expansions of generating exponential functions which are the exact solutions of the initial acoustic and elastodynamic systems. This basis, compared to the classical one based on trigonometric functions, requires less degrees of freedom for the same level of accuracy.

In the present work, we develop the theory for coupled Elasto-Acoustic System (EAS). We confirm well-posedness of the problem, based on the a priory error estimates in mesh dependent norms. We consider a space-time polynomial basis to implement numerically the method and to perform some numerical experiments showing promising results.

Keywords: Trefftz-DG method; elasto-acoustic system; space-time polynomial basis; numerical analysis

AMS Subject Classifications: 65M60; 35Q86; 35L05

1. Introduction

Wave reflection imaging for complex media can be effectively done by using advanced numerical methods (see [4]). In the context of the collaborative research program Depth Imaging Partnership (DIP) between Inria and Total, team-project Magique-3D and Prospective Lab of Houston develop high-order numerical schemes based mostly on discontinuous finite element approximation of wave fields. This technique, known as Discontinuous Galerkin (DG) method, is preferred because it takes into account geometrical and physical features of environment, and it is well-adapted for parallel computation [4, 38]. Recently it has been implemented for coupled elasto-acoustic problems, which led to the development of new propagators in time and frequency domains [39, 40].

However, when comparing to the conventional methods based on continuous approximations, the number of degrees of freedom required by DG method to achieve the same accuracy is significantly higher.

To avoid this difficulty, HDG methods have been developed and their integration into DIP is under way for both acoustic and elastic domains, with the possibility

*Email: elvira.shishenina@inria.fr

of numerical coupling (see [1] and references therein).

Another idea to explore consists in using Trefftz approximation space, whose elements are themselves discrete local solutions of the AS and ES [2, 7]. By its construction, Trefftz methods reduce the number of degrees of freedom, since they require computing surface integrals only to solve the variational formulation. Thus, we may consider the advantages of Trefftz method compared to the standard ones, including better order of convergence, flexible choice of basis functions, low dispersion, local space-time mesh refinement and adaptivity [2, 7].

Trefftz type methods have been widely used with time-harmonic formulations by Farhat, Tezaur, Harari, Hetmaniuk (2003 - 2006) (see [30, 31]), Gabard (2007) (see [32]), Badics (2014) (see [36]), Hiptmair, Moiola, Perugia (2011 - 2013) (see [33–35]) and others, while studies are still limited for reproducing temporal phenomena. Only few papers are interested in Maxwell equations in time [23, 24, 26, 27], but they are mostly devoted to a theoretical analysis of the method, showing the convergence and stability, and numerical tests with plane waves approximation are restricted to 1D + time dimensional case.

Space-time Trefftz approximation by Lagrange multipliers for the second order formulation of the transient wave equation was explored in [25, 28].

Trefftz-DG method for the first-order transient acoustic wave equations in arbitrary space dimensions extending the one-dimensional scheme of Kretzschmar et al. [27] has been introduced in recent paper of Moiola and Perugia (2017) [29]. The authors propose a complete a priori error analysis in both mesh-dependent and mesh-independent norms.

In order to move on numerical simulations of geophysical phenomena and to consider more realistic applications, DIP aims to develop new approximation techniques, which retain DG based methods but operates the Trefftz approach.

In Section 2, we develop a theory for Trefftz-DG method applied to the coupled EAS. We give some a priori error estimates in mesh dependent norms, confirming the well-posedness of the problem. In Section 3, we propose an algorithm of implementation of the method. Some numerical results for 2D simulations will be presented by the end of the Section 3.

2. Space-time Trefftz-DG method

In this Section, we apply Trefftz-DG method for solving first-order elasto-acoustic wave propagation system. We refer to [42] for more theory and demonstrations for the acoustic, elastodynamic and elasto-acoustic problems.

2.1. *Elasto-acoustic wave propagation system*

The elasto-acoustic coupling is motivated by its further numerical application. Indeed, it could be simpler to consider the acoustic media as a limit case of elasto-isotropic media. Thus, it might be possible to solve the elastodynamic problem with variable coefficients, and then, to treat the acoustic medium as a particular region of heterogeneous elastic medium with the shear modulus $\mu \equiv 0$ or very small [21]. However, from a practical point of view, this approach would require computing the six components of stress tensor, instead of the only necessary unknown, that corresponds to the pressure. Moreover, if the numerical code is based on a discretization by H^1 finite elements, the consideration of the limit case $\mu \equiv 0$ would destroy the coercivity in H^1 norms, while a choice of very small μ would

result in numerical artefacts, due to a slow S - waves appearance. An example of this phenomena has been described by Bossy in [16].

Methods, based on discontinuous finite element approximation, are basically well-adapted to specifics of fluid-solid interaction problems. Taking into account the foreseen implementation of the numerical solution in the case of inverse problem, where the goal is to reconstruct media parameters, we consider a transmission problem between the first order elastodynamic and acoustic systems. In the elastodynamic case the problem is solved in terms of velocity-stress, while the acoustic case is considered in terms of velocity-pressure. This choice is seen as more adapted to the imaging conditions and provides straight-forwardly the quantities of interest for the inverse problem.

In this section we introduce EAS based on numerical coupling of proper ES and AS by the transmission conditions, and we develop a space-time Trefftz-DG formulation for the coupled problem. We provide some mesh-dependent error estimates confirming well-posedness of the problem.

2.1.1. Elastodynamic system

The Elastodynamic System of equations is based on three fundamental laws of continuum mechanics: movement equations, constitutive equations (Hooke's law), and geometric equations (infinitesimal strain tensor definition) [14].

We introduce a global space-time domain $Q_S \equiv \Omega_S \times I$, which contains a bounded Lipschitz space domain $\Omega_S \subset R^n$ and a time interval $I \equiv [0, T]$. The Lamé coefficients $\lambda \equiv \lambda(x)$, $\mu \equiv \mu(x)$ and solid density $\rho_S \equiv \rho_S(x)$ are the solid parameters, assumed to be piecewise constant and positive.

We consider the first order ES in solid medium in terms of velocity $v_S \equiv v_S(x,t)$ and stress $\boldsymbol{\sigma} \equiv \boldsymbol{\sigma}(x,t)$ fields:

$$\begin{cases} \dfrac{\partial \boldsymbol{\sigma}}{\partial t} - \boldsymbol{C}\,\boldsymbol{\varepsilon}(v_S) = 0 \text{ in } Q_S, \\ \rho_S \dfrac{\partial v_S}{\partial t} - \mathrm{div}\boldsymbol{\sigma} = 0 \text{ in } Q_S, \\ v_S(\cdot,0) = v_{S0},\ \boldsymbol{\sigma}(\cdot,0) = \boldsymbol{\sigma}_0 \text{ in } \Omega_S, \\ \boldsymbol{\sigma} = \boldsymbol{g}_{D_S} \text{ in } \partial\Omega_S \times I. \end{cases}$$

Here $\boldsymbol{C}$ is the elastic coefficient tensor (symmetrical and positive), $\boldsymbol{\varepsilon}(v_S) = (\nabla v_S + \nabla v_S^T)/2$ is the infinitesimal strain tensor. The boundary conditions $\boldsymbol{g}_{D_S} \equiv \boldsymbol{g}_{D_S}(x,t)$, the velocity v_{s0} and the stress $\boldsymbol{\sigma}_0$ are the initial data.

By symmetry and positivity of the tensor $\boldsymbol{C}$, the application $\boldsymbol{\varepsilon} \longmapsto \boldsymbol{C}\,\boldsymbol{\varepsilon}$ is an isomorphism in the symmetrical tensor space [14]. Thus, we may consider the corresponding inverse application $\boldsymbol{A}$, verifying the same properties of symmetry and positivity:

$$\begin{cases} \boldsymbol{A}\dfrac{\partial\, \boldsymbol{\sigma}}{\partial t} - \boldsymbol{\varepsilon}(v_S) = 0 \text{ in } Q_S, \\ \rho_S \dfrac{\partial v_S}{\partial t} - \mathrm{div}\boldsymbol{\sigma} = 0 \text{ in } Q_S, \\ v_S(\cdot,0) = v_{S0},\ \boldsymbol{\sigma}(\cdot,0) = \boldsymbol{\sigma}_0 \text{ in } \Omega_S, \\ \boldsymbol{\sigma}_S = \boldsymbol{g}_{D_S} \text{ in } \partial\Omega_S \times I. \end{cases} \tag{1}$$

2.1.2. Acoustic system

To consider an initial boundary value problem in inviscid fluid media, we introduce a global space-time domain $Q_F \equiv \Omega_F \times I$, where $\Omega_F \subset R^n$ is a bounded Lipschitz space domain, and a time interval $I \equiv [0, T]$. The fluid parameters $c_F \equiv c_F(x)$ and $\rho_F \equiv \rho_F(x)$, standing for the acoustic wave propagation velocity and fluid density respectively, piecewise constant and positive.

We consider the first order AS in terms of velocity $v_F \equiv v_F(x,t)$ and pressure $p \equiv p(x,t)$ fields:

$$\begin{cases} \dfrac{1}{c_F^2 \rho_F} \dfrac{\partial p}{\partial t} + \mathrm{div} v_F = f \text{ in } Q_F, \\ \rho_F \dfrac{\partial v_F}{\partial t} + \nabla p = 0 \text{ in } Q_F, \\ v_F(\cdot, 0) = v_{F0},\ p(\cdot, 0) = p_0 \text{ in } \Omega_F, \\ v_F = \mathrm{g}_{D_F} \text{ in } \partial\Omega_F \times I. \end{cases} \tag{2}$$

The source function $f \equiv f(x,t)$, the boundary term $\mathrm{g}_{D_F} \equiv \mathrm{g}_{D_F}(x,t)$, and the velocity v_{F0} and pressure p_0 are the direct problem data.

2.1.3. Transmission conditions

The choice of the transmission conditions requires the continuity of velocity and stress normal components at the interface $\Gamma_{FS} \equiv \partial\Omega_F \cap \partial\Omega_S$. The velocities aligned to the interface and the tangential stress remain unconstrained [14, 15]:

$$\begin{cases} v_F \cdot n_{\Gamma_{FS}} = v_S \cdot n_{\Gamma_{FS}} \text{ at } \Gamma_{FS}, \\ \boldsymbol{\sigma} n_{\Gamma_{FS}} = -p n_{\Gamma_{FS}} \text{ at } \Gamma_{FS}, \end{cases} \tag{3}$$

where $n_{\Gamma_{FS}}$ is a unit normal vector to Γ_{FS}, outwardly directed to Ω_F. We will apply (3) to the in-coming and out-going flux terms at Γ_{FS} to couple acoustic and elastodynamic formulations.

2.2. *Space-time DG formulation*

We introduce a non-overlapping space-time mesh $\mathcal{T}_h \equiv \{K_F\} \cup \{K_S\}$ of Lipschitz elements $K_S \subset Q_S$, $K_F \subset Q_F$ on the global space $Q \equiv Q_F \cup Q_S$. Let $n_{K_S} \equiv (n^x_{K_S}, n^t_{K_S})$, $n_{K_F} \equiv (n^x_{K_F}, n^t_{K_F})$ the outward pointing unit normal vectors on ∂K_S and ∂K_F respectively. Without losing generality with respect to the classical space DG methods, we start with the particular cases of meshes, whose elements are right prisms, with vertical sides parallel to time axis. We consider all media parameters to be constant in K_S, K_F. Unknowns v_S, $\boldsymbol{\sigma}$, v_F and p are supposed to be in $H^1(K_S)^d$, $H^1(K_S)^{d^2}$, $H^1(K_F)^d$ and $H^1(K_F)$ respectively, where d is dimension of physical space $\Omega \equiv \Omega_F \cup \Omega_S$.

Multiplying the equations of (1) by the test functions $\boldsymbol{\xi} \in H^1(K_S)^{d^2}$ and $\omega_S \in H^1(K_S)^d$, the equations of (2) by the test functions $q \in H^1(K_F)$ and $\omega_F \in H^1(K_F)^d$, and integrating by part in time and space, we obtain:

$$
\begin{aligned}
&-\int_{K_S}\Big[\boldsymbol{\sigma}:(\boldsymbol{A}\frac{\partial\boldsymbol{\xi}}{\partial t}-\boldsymbol{\varepsilon}(\omega_S))+v_S\cdot(\rho_S\frac{\partial\omega_S}{\partial t}-\mathrm{div}\boldsymbol{\xi})\Big]d\mathrm{v}\\
&+\int_{\partial K_S}\Big[\boldsymbol{A}\,\boldsymbol{\sigma}:\boldsymbol{\xi}n^t_{K_S}-v_S\cdot n^x_{K_S}\boldsymbol{\xi}+\rho_S v_S n^t_{K_S}\cdot\omega_S-\boldsymbol{\sigma}n^x_{K_S}\cdot\omega_S\Big]d\mathrm{s}=0,\\
&-\int_{K_F}\Big[p(\frac{1}{c_F^2\rho_F}\frac{\partial q}{\partial t}+\mathrm{div}\omega_F)+v_F\cdot(\rho_F\frac{\partial\omega_F}{\partial t}+\nabla q)\Big]d\mathrm{v}\\
&+\int_{\partial K_F}\Big[\frac{1}{c_F^2\rho_F}pn^t_{K_F}q+v_F\cdot n^x_{K_F}q+\rho_F v_F n^t_{K_F}\cdot\omega_F+pn^x_{K_F}\cdot\omega_F\Big]d\mathrm{s}=\int_{K_F}fqd\mathrm{v}.
\end{aligned}
$$

Since the space-time mesh has been introduced, the mesh skeleton $\mathcal{F}_h=[\cup_{K_S\in\mathcal{T}_h}\partial K_S]\cup[\cup_{K_F\in\mathcal{T}_h}\partial K_F]$ can be decomposed into families of element faces as follows [27]:

$$
\begin{aligned}
\mathcal{F}_h^{\Omega_S}&-\text{ internal }\Omega\text{-faces in solid }(t\text{ - fixed}),\\
\mathcal{F}_h^{I_S}&-\text{ internal }I\text{-faces in solid }(x\text{ - fixed}),\\
\mathcal{F}_h^{0_S}&-\text{ external initial time faces }(\Omega_S\times\{0\}),\\
\mathcal{F}_h^{T_S}&-\text{ external final time faces }(\Omega_S\times\{T\}),\\
\mathcal{F}_h^{D_S}&-\text{ external Dirichlet boundary faces }(\partial\Omega_S\times[0,T]),\\
\mathcal{F}_h^{\Omega_F}&-\text{ internal }\Omega\text{-faces in fluid }(t\text{ - fixed}),\\
\mathcal{F}_h^{I_F}&-\text{ internal }I\text{-faces in fluid }(x\text{ - fixed})\\
\mathcal{F}_h^{0_F}&-\text{ external initial time faces }(\Omega_F\times\{0\}),\\
\mathcal{F}_h^{T_F}&-\text{ external final time faces }(\Omega_F\times\{T\}),\\
\mathcal{F}_h^{D_F}&-\text{ external Dirichlet boundary faces }(\partial\Omega_F\times[0,T]),\\
\mathcal{F}_h^{FS}&-\text{ internal fluid-solid interface faces }(\Gamma_{FS}\times[0,T]).
\end{aligned}
$$

To fix the notations, we define the averages $\{\!\{\cdot\}\!\}$, space normal jumps $[\![\cdot]\!]_x$ and time jumps $[\![\cdot]\!]_t$ between two elements $K^1_{F,S}$ and $K^2_{F,S}$ for piecewise-continuous scalar p, vector $v_{F,S}$ and tensor $\boldsymbol{\sigma}$ fields [4]:

$$
\begin{aligned}
&\{\!\{p\}\!\}\equiv\frac{1}{2}(p_{|K^1_F}+p_{|K^2_F}) && \text{on } \partial K^1_F\cap\partial K^2_F\subset\mathcal{F}_h^{I_F},\\
&[\![p]\!]_x\equiv p_{|K^1_F}n^x_{K^1_F}+p_{|K^2_F}n^x_{K^2_F} && \text{on } \partial K^1_F\cap\partial K^2_F\subset\mathcal{F}_h^{I_F},\\
&[\![p]\!]_t\equiv p_{|K^1_F}n^t_{K^1_F}+p_{|K^2_F}n^t_{K^2_F} && \text{on } \partial K^1_F\cap\partial K^2_F\subset\mathcal{F}_h^{\Omega_F},\\
&\{\!\{v_{F,S}\}\!\}\equiv\frac{1}{2}(v_{F,S|K^1_{F,S}}+v_{F,S|K^2_{F,S}}) && \text{on } \partial K^1_{F,S}\cap\partial K^2_{F,S}\subset\mathcal{F}_h^{I_F},\\
&[\![v_{F,S}]\!]_x\equiv v_{F,S|K^1_{F,S}}\cdot n^x_{K^1_{F,S}}+v_{F,S|K^2_{F,S}}\cdot n^x_{K^2_{F,S}} && \text{on } \partial K^1_{F,S}\cap\partial K^2_{F,S}\subset\mathcal{F}_h^{I_F},\\
&[\![v_{F,S}]\!]_t\equiv v_{F,S|K^1_{F,S}}n^t_{K^1_{F,S}}+v_{F,S|K^2_{F,S}}n^t_{K^2_{F,S}} && \text{on } \partial K^1_{F,S}\cap\partial K^2_{F,S}\subset\mathcal{F}_h^{\Omega_F},
\end{aligned}
$$

$$
\begin{aligned}
\{\!\{\boldsymbol{\sigma}\}\!\} &\equiv \frac{1}{2}(\boldsymbol{\sigma}_{|K_S^1} + \boldsymbol{\sigma}_{|K_S^2}) && \text{on } \partial K_S^1 \cap \partial K_S^2 \subset \mathcal{F}_h^{I_F},\\
[\![\boldsymbol{\sigma}]\!]_x &\equiv \boldsymbol{\sigma}_{|K_S^1} n^x_{K_S^1} + \boldsymbol{\sigma}_{|K_S^2} n^x_{K_S^2} && \text{on } \partial K_S^1 \cap \partial K_S^2 \subset \mathcal{F}_h^{I_F},\\
[\![\boldsymbol{\sigma}]\!]_t &\equiv \boldsymbol{\sigma}_{|K_F^1} n^t_{K_S^1} + \boldsymbol{\sigma}_{|K_S^2} n^t_{K_S^2} && \text{on } \partial K_S^1 \cap \partial K_S^2 \subset \mathcal{F}_h^{\Omega_F}.
\end{aligned}
$$

We also use the superscripts "$-$" and "$+$" to refer to the interior and the exterior information respectively for each element [4].

The space-time DG discretization of the coupled problem consists in finding $(v_{Fh}, p_h, v_{Sh}, \boldsymbol{\sigma}_h) \subset H^1(\mathcal{T}_h)^d \times H^1(\mathcal{T}_h) \times H^1(\mathcal{T}_h)^d \times H^1(\mathcal{T}_h)^{d^2}$ such that, for all $(\omega_F, q, \omega_S, \boldsymbol{\xi}) \subset H^1(\mathcal{T}_h)^d \times H^1(\mathcal{T}_h) \times H^1(\mathcal{T}_h)^d \times H^1(\mathcal{T}_h)^{d^2}$ and for all $K_F, K_S \in \mathcal{T}_h$ it holds:

$$
\begin{aligned}
&-\int_{K_S} \Big[\boldsymbol{\sigma}_h : (\boldsymbol{A}\frac{\partial\, \boldsymbol{\xi}}{\partial t} - \boldsymbol{\varepsilon}(\omega_S)) + v_{Sh} \cdot (\rho_S \frac{\partial \omega_S}{\partial t} - \mathrm{div}\boldsymbol{\xi})\Big] d\mathrm{v}\\
&+\int_{\partial K_S} \Big[\boldsymbol{A}\,\hat{\boldsymbol{\sigma}}_h : \boldsymbol{\xi} n^t_{K_S} - v_{\hat{S}h} \cdot n^x_{K_S}\boldsymbol{\xi} + \rho_S v_{\hat{S}h} n^t_{K_S} \cdot \omega_S - \hat{\boldsymbol{\sigma}}_h n^x_{K_S} \cdot \omega_S\Big] d\mathrm{s} = 0,\\
&-\int_{K_F} \Big[p_h(\frac{1}{c_F^2 \rho_F}\frac{\partial q}{\partial t} + \mathrm{div}\omega_F) + v_{Fh} \cdot (\rho_F \frac{\partial \omega_F}{\partial t} + \nabla q)\Big] d\mathrm{v}\\
&+\int_{\partial K_F} \Big[\frac{1}{c_F^2 \rho_F}\hat{p_h} n^t_{K_F} q + v_{\hat{F}h} \cdot n^x_{K_F} q + \rho_F v_{\hat{F}h} n^t_{K_F} \cdot \omega_F + \hat{p_h} n^x_{K_F} \cdot \omega_F\Big] d\mathrm{s} = \int_{K_F} f q d\mathrm{v},
\end{aligned}
$$

where numerical fluxes $v_{\hat{F}h}$, $\hat{p_h}$, $v_{\hat{S}h}$, $\hat{\boldsymbol{\sigma}}_h$ are defined on the mesh skeleton $\mathcal{F}_h$ as following:

$$
\begin{aligned}
\begin{pmatrix} v_{\hat{F}h} \\ \hat{p_h} \end{pmatrix} &\equiv \begin{pmatrix} \{\!\{v_{Fh}\}\!\} + \beta [\![p_h]\!]_x \\ \{\!\{p_h\}\!\} + \alpha [\![v_{Fh}]\!]_x \end{pmatrix} && \text{on } \mathcal{F}_h^{I_F},\\
\begin{pmatrix} v_{\hat{S}h} \\ \hat{\boldsymbol{\sigma}}_h \end{pmatrix} &\equiv \begin{pmatrix} \{\!\{v_{Sh}\}\!\} - \delta [\![\boldsymbol{\sigma}_h]\!]_x \\ \{\!\{\boldsymbol{\sigma}_h\}\!\} - \gamma [\![v_{Sh}]\!]_x \end{pmatrix} && \text{on } \mathcal{F}_h^{I_S},\\
\begin{pmatrix} v_{\hat{F}h} \cdot n^x_{K_F} \\ \hat{p_h} n^x_{K_F} \end{pmatrix} &\equiv \begin{pmatrix} \mathrm{g}_{D_F} \cdot n^x_{K_F} \\ p_h n^x_{K_F} + \alpha(v_{Fh} - \mathrm{g}_{D_F}) \cdot n^x_{K_F} \end{pmatrix} && \text{on } \mathcal{F}_h^{D_F},\\
\begin{pmatrix} v_{\hat{S}h} \cdot n^x_{K_S} \\ \hat{\boldsymbol{\sigma}}_h n^x_{K_S} \end{pmatrix} &\equiv \begin{pmatrix} v_{Sh} \cdot n^x_{K_S} - \delta(\boldsymbol{\sigma}_h - \boldsymbol{g}_{D_S}) n^x_{K_S} \\ \boldsymbol{g}_{D_S} n^x_{K_S} \end{pmatrix} && \text{on } \mathcal{F}_h^{D_S},\\
\begin{pmatrix} v_{\hat{F}h} \\ \hat{p_h} \end{pmatrix} &\equiv \begin{pmatrix} {v_{Fh}}^- \\ {p_h}^- \end{pmatrix} && \text{on } \mathcal{F}_h^{\Omega_F},\\
\begin{pmatrix} v_{\hat{S}h} \\ \hat{\boldsymbol{\sigma}}_h \end{pmatrix} &\equiv \begin{pmatrix} {v_{Sh}}^- \\ {\boldsymbol{\sigma}_h}^- \end{pmatrix} && \text{on } \mathcal{F}_h^{\Omega_S},\\
\begin{pmatrix} v_{\hat{F}h} \\ \hat{p_h} \end{pmatrix} &\equiv \begin{pmatrix} v_{Fh} \\ p_h \end{pmatrix} && \text{on } \mathcal{F}_h^{T_F},\\
\begin{pmatrix} v_{\hat{S}h} \\ \hat{\boldsymbol{\sigma}}_h \end{pmatrix} &\equiv \begin{pmatrix} v_{Sh} \\ \boldsymbol{\sigma}_h \end{pmatrix} && \text{on } \mathcal{F}_h^{T_S},\\
\begin{pmatrix} v_{\hat{F}h} \\ \hat{p_h} \end{pmatrix} &\equiv \begin{pmatrix} v_{F0} \\ p_0 \end{pmatrix} && \text{on } \mathcal{F}_h^{0_F},\\
\begin{pmatrix} v_{\hat{S}h} \\ \hat{\boldsymbol{\sigma}}_h \end{pmatrix} &\equiv \begin{pmatrix} v_{S0} \\ \boldsymbol{\sigma}_0 \end{pmatrix} && \text{on } \mathcal{F}_h^{0_S},
\end{aligned}
$$

$$\begin{pmatrix} v\hat{_{Fh}} \cdot n^x_{K_F} \\ \hat{p_h} n^x_{K_F} \\ v\hat{_{Sh}} \cdot n^x_{K_S} \\ \hat{\boldsymbol{\sigma}_h} n^x_{K_S} \end{pmatrix} \equiv \begin{pmatrix} v_{Sh} \cdot n^x_{K_F} \\ p_h n^x_{K_F} + \alpha(v_{Fh} - v_{Sh}) \cdot n^x_{K_F} \\ v_{Sh} \cdot n^x_{K_S} - \delta(\boldsymbol{\sigma}_h - p_h) n^x_{K_S} \\ -p_h n^x_{K_S} \end{pmatrix} \quad \text{on } \mathcal{F}_h^{FS}.$$

2.3. *Trefftz-DG formulation*

We define the Trefftz space in the elasto-acoustic medium, such that the chosen test functions ω_S, $\boldsymbol{\xi}$ and ω_F, q satisfy respectively the elastodynamic and acoustic equations inside each element K_S and K_F:

$$\begin{aligned} \mathbf{T}(\mathcal{T}_h) \equiv \Big\{ & (\omega_F, q, \omega_S, \boldsymbol{\xi}) \subset H^1(\mathcal{T}_h)^d \times H^1(\mathcal{T}_h) \times H^1(\mathcal{T}_h)^d \times H^1(\mathcal{T}_h)^{d^2} \text{ s. t.} \\ & \rho_F \frac{\partial \omega_F}{\partial t} + \nabla q = \frac{1}{c_F^2 \rho_F} \frac{\partial q}{\partial t} + \mathrm{div} \omega_F = 0 \text{ in all } K_F \in \mathcal{T}_h, \\ & \rho_S \frac{\partial \omega_S}{\partial t} - \mathrm{div} \boldsymbol{\xi} = \frac{\partial \boldsymbol{A}\, \boldsymbol{\xi}}{\partial t} - \boldsymbol{\varepsilon}(\omega_S) = 0 \text{ in all } K_S \in \mathcal{T}_h \Big\}. \end{aligned}$$

This choice of basis functions removes all volume integral terms in the DG formulation above. Thus Trefftz-DG formulation for EAS reads as:

Seek $(v_{Fh}, p_h, v_{Sh}, \boldsymbol{\sigma}_h) \subset \mathbf{T}(\mathcal{T}_h)$ *s.t., for all* $(\omega_F, q, \omega_S, \boldsymbol{\xi}) \subset \mathbf{T}(\mathcal{T}_h)$, *it holds true:*

$$\begin{aligned} & \int_{\mathcal{F}_h^{\Omega_S}} \Big[\boldsymbol{A}\, \boldsymbol{\sigma}_h{}^- : [\![\boldsymbol{\xi}]\!]_t + \rho_S v_{Sh}{}^- [\![\omega_S]\!]_t \Big] \mathrm{d}s \\ & - \int_{\mathcal{F}_h^{I_S}} \Big[\{\!\{ \boldsymbol{\sigma}_h \}\!\} [\![\omega_S]\!]_x + \{\!\{ v_{Sh} \}\!\} [\![\boldsymbol{\xi}]\!]_x - \gamma [\![v_{Sh}]\!]_x [\![\omega_S]\!]_x - \delta [\![\boldsymbol{\sigma}_h]\!]_x [\![\boldsymbol{\xi}]\!]_x \Big] d\mathrm{s} \\ & + \int_{\mathcal{F}_h^{T_S}} \Big[\boldsymbol{A}\, \boldsymbol{\sigma}_h : \boldsymbol{\xi} + \rho_S v_{Sh} \cdot \omega_S \Big] d\mathrm{s} - \frac{1}{2} \int_{\mathcal{F}_h^{0_S}} \Big[\boldsymbol{A}\, \boldsymbol{\sigma}_h : \boldsymbol{\xi} + \rho_S v_{Sh} \cdot \omega_S \Big] d\mathrm{s} \\ & - \int_{\mathcal{F}_h^{D_S}} \Big[v_{Sh} \cdot n^x_{K_S} \boldsymbol{\xi} - \delta \boldsymbol{\sigma}_h : \boldsymbol{\xi} \Big] d\mathrm{s} \\ & - \int_{\mathcal{F}_h^{FS}} \Big[v_{Sh} \cdot n^x_{K_S} \boldsymbol{\xi} - \delta (\boldsymbol{\sigma}_h n^x_{K_S} - p_h n^x_{K_S}) \boldsymbol{\xi} - p n^x_{K_S} \cdot \omega_S \Big] d\mathrm{s} = \\ & \frac{1}{2} \int_{\mathcal{F}_h^{0_S}} \Big[\boldsymbol{A}\, \boldsymbol{\sigma}_h : \boldsymbol{\xi} + \rho_S v_{Sh} \cdot \omega_S \Big] d\mathrm{s} + \int_{\mathcal{F}_h^{D_S}} \Big[\boldsymbol{g}_{D_S} n^x_{K_S} \cdot \omega_S + \delta \boldsymbol{g}_{D_S} : \boldsymbol{\xi}) \Big] d\mathrm{s}, \end{aligned}$$

$$\begin{aligned} & \int_{\mathcal{F}_h^{\Omega_F}} \Big[\frac{1}{c_F^2 \rho_F} p_h{}^- [\![q]\!]_t + \rho_F v_{Fh}{}^- [\![\omega_F]\!]_t \Big] d\mathrm{s} \\ & + \int_{\mathcal{F}_h^{I_F}} \Big[\{\!\{ p_h \}\!\} [\![\omega_F]\!]_x + \{\!\{ v_{Fh} \}\!\} [\![q]\!]_x + \alpha [\![v_{Fh}]\!]_x [\![\omega_F]\!]_x + \beta [\![p_h]\!]_x [\![q]\!]_x \Big] d\mathrm{s} \\ & + \int_{\mathcal{F}_h^{T_F}} \Big[\frac{1}{c_F^2 \rho_F} p_h n^t_{K_F} q + \rho_F v_{Fh} n^t_{K_F} \cdot \omega_F \Big] d\mathrm{s} \\ & - \frac{1}{2} \int_{\mathcal{F}_h^{0_F}} \Big[\frac{1}{c_F^2 \rho_F} p_h n^t_{K_F} q + \rho_F v_{Fh} n^t_{K_F} \cdot \omega_F \Big] d\mathrm{s} + \int_{\mathcal{F}_h^{D_F}} \Big[p n^x_{K_F} \cdot \omega_F + \alpha v_{Fh} \cdot \omega_F \Big] d\mathrm{s} \end{aligned}$$

$$+\int_{\mathcal{F}_h^{FS}}\Big[p_h n^x_{K_F}\cdot\omega_F+\alpha(v_{Fh}\cdot n^x_{K_F}-v_{Sh}\cdot n^x_{K_F})\cdot\omega_F+v_{Sh}\cdot n^x_{K_F}q)\Big]d\mathrm{s}=$$
$$\frac{1}{2}\int_{\mathcal{F}_h^{0_F}}\Big[\frac{1}{c_F^2\rho_F}p_h q+\rho_F v_{Fh}\cdot\omega_F\Big]d\mathrm{s}+\int_{\mathcal{F}_h^{D_F}}\Big[\alpha \mathrm{g}_{D_F}\cdot\omega_F-\mathrm{g}_{D_F}\cdot n^x_{K_F}q\Big]d\mathrm{s},$$

which can be rewritten, using bilinear $\mathcal{A}_{TDG}(\cdot\,;\cdot)$ and linear $\ell_{TDG}(\cdot)$ operators, as following:

Seek $(v_{Fh},p_h,v_{Sh},\boldsymbol{\sigma}_h)\subset\mathbf{T}(\mathcal{T}_h)$ *s.t., for all* $(\omega_F,q,\omega_S,\boldsymbol{\xi})\subset\mathbf{T}(\mathcal{T}_h)$, *it holds true:*

$$\mathcal{A}_{TDG}((v_{Fh},p_h,v_{Sh},\boldsymbol{\sigma}_h);(\omega_F,q,\omega_S,\boldsymbol{\xi}))=\ell_{TDG}(\omega_F,q,\omega_S,\boldsymbol{\xi}). \tag{4}$$

2.4. *Well-posedness*

We refer to the estimates, obtained previously for the acoustic, elastic and coupled elasto-acoustic problems in [42]. The analysis is carried out in the framework developed in [27] for the time-dependent Maxwell problem.

We introduce two mesh-dependent semi-norms $|||\cdot|||^2_{TDG}$ and $|||\cdot|||^2_{TDG^*}$ as follows:

$$|||(\omega_F,q,\omega_S,\boldsymbol{\xi})|||^2_{TDG}\equiv\frac{1}{2}\Big\|(\boldsymbol{A})^{1/2}[\![\boldsymbol{\xi}]\!]_t\Big\|^2_{L^2(\mathcal{F}_h^{\Omega_S})}+\frac{1}{2}\Big\|\rho_S^{1/2}[\![\omega_S]\!]_t\Big\|^2_{L^2(\mathcal{F}_h^{\Omega_S})}$$
$$+\Big\|\gamma^{1/2}[\![\omega_S]\!]_x\Big\|^2_{L^2(\mathcal{F}_h^{I_S})}+\Big\|\delta^{1/2}[\![\boldsymbol{\xi}]\!]_x\Big\|^2_{L^2(\mathcal{F}_h^{I_S})}+\frac{1}{2}\Big\|(\boldsymbol{A})^{1/2}\boldsymbol{\xi}\Big\|^2_{L^2(\mathcal{F}_h^{T_S})}$$
$$+\frac{1}{2}\Big\|\rho_S^{1/2}\omega_S\Big\|^2_{L^2(\mathcal{F}_h^{T_S})}+\Big\|\delta^{1/2}\boldsymbol{\xi}\Big\|^2_{L^2(\mathcal{F}_h^{D_S})}+2\|\delta^{1/2}\boldsymbol{\xi}\|^2_{L^2(\mathcal{F}_h^{FS})}+\Big\|\alpha^{1/2}\omega_F\|^2_{L^2(\mathcal{F}_h^{D_F})}$$
$$+\frac{1}{2}\Big\|(\frac{1}{c_F^2\rho_F})^{1/2}[\![q]\!]_t\Big\|^2_{L^2(\mathcal{F}_h^{\Omega_F})}+\frac{1}{2}\Big\|\rho_F^{1/2}[\![\omega_F]\!]_t\Big\|^2_{L^2(\mathcal{F}_h^{\Omega_F})}+\Big\|\alpha^{1/2}[\![\omega_F]\!]_x\Big\|^2_{L^2(\mathcal{F}_h^{I_F})}$$
$$+\Big\|\beta^{1/2}[\![q]\!]_x\Big\|^2_{L^2(\mathcal{F}_h^{I_F})}+\frac{1}{2}\Big\|(\frac{1}{c_F^2\rho_F})^{1/2}q\Big\|^2_{L^2(\mathcal{F}_h^{T_F})}+\frac{1}{2}\Big\|\rho_F^{1/2}\omega_F\Big\|^2_{L^2(\mathcal{F}_h^{T_F})},$$

$$|||(\omega_F,q,\omega_S,\boldsymbol{\xi})|||^2_{TDG^*}\equiv|||(\omega_F,q,\omega_S,\boldsymbol{\xi})|||^2_{TDG}+\|\rho_S^{1/2}\omega_S^-\|^2_{L^2(\mathcal{F}_h^{\Omega_S})}$$
$$+\|(\boldsymbol{A})^{1/2}\boldsymbol{\xi}^-\|^2_{L^2(\mathcal{F}_h^{\Omega_S})}+\|\delta^{-1/2}\{\!\{\omega_S\}\!\}\|^2_{L^2(\mathcal{F}_h^{I_S})}+\|\gamma^{-1/2}\{\!\{\boldsymbol{\xi}\}\!\}\|^2_{L^2(\mathcal{F}_h^{I_S})}$$
$$+\|\delta^{-1/2}\boldsymbol{\xi}\|^2_{L^2(\mathcal{F}_h^{D_S})}+\frac{1}{2}\|\alpha^{-1/2}\boldsymbol{\xi}\|^2_{L^2(\mathcal{F}_h^{FS})}+\|\alpha^{-1/2}\omega_F\|^2_{L^2(\mathcal{F}_h^{D_F})}+\|\rho_F^{1/2}\omega_F^-\|^2_{L^2(\mathcal{F}_h^{\Omega_F})}$$
$$+\|(\frac{1}{c_F^2\rho_F})^{1/2}q^-\|^2_{L^2(\mathcal{F}_h^{\Omega_F})}+\|\beta^{-1/2}\{\!\{\omega_F\}\!\}\|^2_{L^2(\mathcal{F}_h^{I_F})}+\|\alpha^{-1/2}\{\!\{q\}\!\}\|^2_{L^2(\mathcal{F}_h^{I_F})}.$$

Using these semi-norms, the coercivity and continuity properties of bilinear $\mathcal{A}_{TDG}(\cdot,\cdot)$ and linear $\ell_{TDG}(\cdot)$ forms hold true:

$$\mathcal{A}_{TDG}((\omega_F,q,\omega_S,\boldsymbol{\xi});(\omega_F,q,\omega_S,\boldsymbol{\xi}))=|||(\omega_F,q,\omega_S,\boldsymbol{\xi})|||^2_{TDG},$$

$$|\mathcal{A}_{TDG}((v_F,p,v_S,\boldsymbol{\sigma});(\omega_F,q,\omega_S,\boldsymbol{\xi}))| \le 2\,|||(v_F,p,v_S,\boldsymbol{\sigma})|||_{TDG^*}\,|||(\omega_F,q\omega_S,\boldsymbol{\xi})|||_{TDG},$$

$$|\ell_{TDG}(v_F,p,v_S,\boldsymbol{\sigma})| \le \sqrt{2}\,\Big[\|\rho_F^{1/2}v_{F0}\|^2_{L^2(\mathcal{F}_h^{0_F})} + \|(\frac{1}{c_F^2\rho_F})^{1/2}p_0\|^2_{L^2(\mathcal{F}_h^{0_F})}$$
$$+\ \|\rho_S^{1/2}v_{S0}\|^2_{L^2(\mathcal{F}_h^{0_S})} + \|\boldsymbol{A}^{1/2}\boldsymbol{\sigma}_0\|^2_{L^2(\mathcal{F}_h^{0_S})}\Big]^{1/2}, \quad (\mathrm{g}_{D_F} = \boldsymbol{g}_{D_S} \equiv 0),$$

It can be simply shown that the semi-norms $|||\cdot|||_{TDG}$ and $|||\cdot|||_{TDG^*}$ are norms on the space $\mathbf{T}(\mathcal{T}_h)$. The demonstration is similar to the technique proposed in [27] for the first order Maxwell equation. Regarding the Lax-Milgram theorem, these estimates prove that the variational problem (4) admits a unique weak solution $(v_{Fh},p_h,v_{Sh},\boldsymbol{\sigma}_h) \in \mathbf{T}(\mathcal{T}_h)$, with

$$|||(v_F - v_{Fh}, p - p_h, v_F - v_{Fh}, p - p_h)|||_{TDG} \le$$
$$3 \inf_{(\omega_F,q,\omega_S,\boldsymbol{\xi})\in\mathbf{T}(\mathcal{T}_h)} |||(v_F-\omega_F, p-q, v_S-\omega_S, \boldsymbol{\sigma}-\boldsymbol{\xi})|||_{TDG^*}.$$

3. Implementation of the method

In this Section we consider a simple example of a one-dimensional homogeneous medium, in order to better understand the method implementation. We briefly introduce the choice of polynomial basis (we refer the reader to the Appendix B of [42] for more numerical details on the algorithm of polynomial basis computing as well as for basis examples in 2D acoustics and elastodynamics). In the end of the Section we give some results of 2D simulations for the acoustic, elastodynamic and coupled elasto-acoustic problems.

3.1. *Numerical algorithm*

We choose a one-dimensional space domain $\Omega \equiv [x_L, x_R]$ and a time domain $I \equiv [0,T]$ so that $Q \equiv \Omega \times I$ represents a rectangle.

The uniform mesh $\mathcal{T}_h$ on Q is composed of non-overlapping rectangular elements $K^k,\ k = 1,..N_{el},\ N_{el} = N_x \times N_t$, with edges parallel to the space and time axes, and equal to $\Delta x = (x_R - x_L)/N_x$ and $\Delta t = T/N_t$ respectively (see Figure 1).

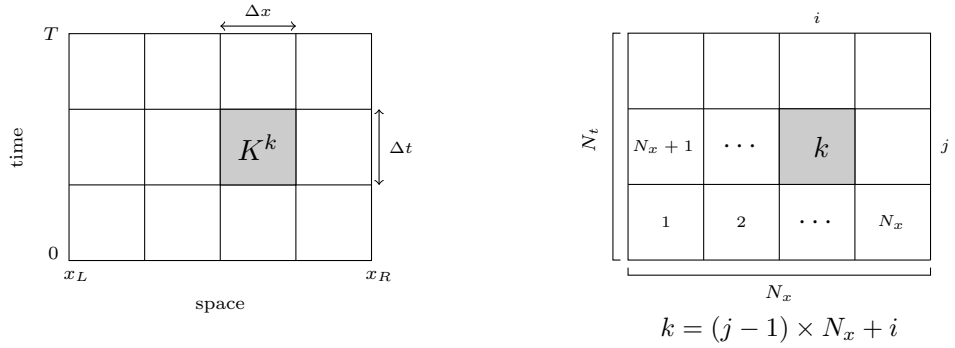

Figure 1. Uniform rectangular mesh $\mathcal{T}_h$ on Q. Element numbering.

Once we have defined the discrete approximation space, we can solve the problem inside each element K, communicating values at the boundaries ∂K by the incoming and out-going fluxes. Thus, the variational problem will be represented

by a global algebraic linear system, with a global sparse matrix, of size equals to the total number of elements multiplied by the number of degrees of freedom per element ($N_t \times N_x \times$ ndof). The inversion of a huge matrix, numerically speaking, is a very expensive process. In order to optimize the execution of the algorithm, we will solve the problem "layer by layer", considering final results, computed on the current time layer at time t, as initial values for the next layer at time $t + \Delta t$ (see Figure 2).

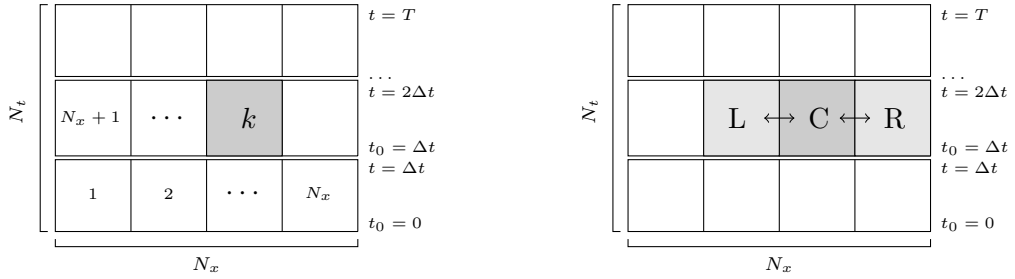

Figure 2. Uniform rectangular mesh $\mathcal{T}_h$ on Q. Decomposing on layers.

It means, that inside each time slab we solve the formulation inside each element, taking into account in-coming and out-going fluxes from its two neighbours (left and right ones). Thus, the global matrix will have a block tridiagonal form, of size N_t times smaller than the original one (see Figure 3).

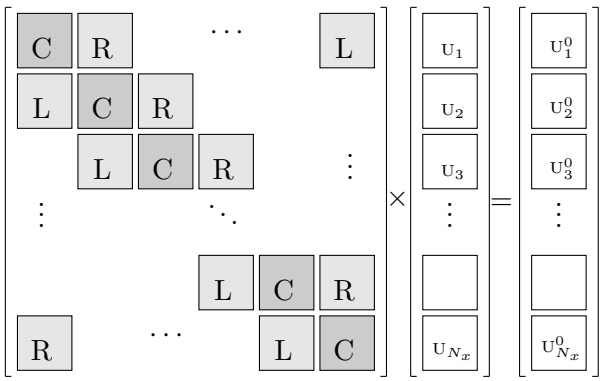

Figure 3. Global algebraic linear system with block tridiagonal matrix.

One more feature to reduce the numerical costs consists in computing space and time integrals on faces of one element of reference (unit square), and then, in projecting the computed values to all mesh elements (multiplying by Δx and Δt for space and time integration respectively in the case of rectangular mesh).

To sum up, we propose a short pseudo-code, which describes the algorithm of the method implementation. It is important to notice, that the main loop in time contains three steps:

1) computation of the approximation coefficients u for the numerical solution in the current time slab $[t_{j-1}, t_j]$;

2) computation of the intermediate numerical solutions v and p thanks to the approximation coefficients u at the end of the current time slab t_j, using *tsnap* function, which computes the trace of numerical solution at time t_j.

3) reinitialization of the initial values - computation of the right-hand side u0=0.5(v0+p0) at the beginning t_j of the next time slab $[t_j, t_{j+1}]$, thanks to the intermediate numerical solutions v and p from the step 2, using the L^2-projection function *l2proj*.

Data: vt0, pt0 % initial velocity and pressure fields
c, rho, space, time % domain parameters
dx, dt, nx, nt, ndf % mesh and DG parameters
Result: v_tfin, p_tfin % final velocity and pressure fields
Compute:
v0=$l2proj$(vt0, phi_v) % velocity and pressure linear terms at $t_0 = 0$
p0=$l2proj$(pt0, phi_p)
u0=0.5(v0+p0) % initial right-hand side
M % global sparse matrix - left-hand side
invM = M^{-1} % inversion of the global matrix
for $j = 1 : nt$ **do**
  Compute:
  u = invM*u0 % vector of the coefficients for approximate
  % solution in the time slab $[(j-1)$dt, $j$dt$]$
  v=$tsnap$(u, phi_v, t_j) % intermediate approximate solutions for velocity
  p=$tsnap$(u, phi_p, t_j) % and pressure fields at $t_j = j$dt
  v0=$l2proj$(v, phi_v) % intermediate velocity and pressure linear
  p0=$l2proj$(p, phi_p) % terms at $t_j = j$dt
  u0=0.5(v0+p0) % reinitialization of the right-hand side
end
Compute:
v_tfin=$tsnap$(u, phi_v, t_{nt}) % final approximate solutions for velocity and
p_tfin=$tsnap$(u, phi_p, t_{nt}) % pressure fields at $t_{nt} = nt$dt

The idea to remove the last two steps, corresponding to the "projection" of the approximation coefficients to the numerical solution, is quite attractive, because it will provide a faster implementation of the code (we could reuse directly a vector of approximation coefficients computed in the previous slab).

In order to explore this idea we have employed the algorithm introduced by Antonietti and Mazzieri in [37]. This algorithm is based on a space semi-discretization of second order hyperbolic problems that results in a high-order DG scheme. Using DG spectral element approach the authors provide an implicit high-order time integration scheme. The obtained scheme possess an important property: the solution at given time slab $[t_j, t_{j+1}]$ depends only on the solution at t_j^- (that is not the case for the finite difference schemes where previous steps have to be taken into account).

In order to adapt the developed scheme to the method, described by the authors [37], we had to replace the numerical fluxes $v_{\hat{F}h}$, $\hat{p_h}$, $v_{\hat{S}h}$, $\hat{\boldsymbol{\sigma}}_h$ by the central ones, to obtain completely symmetrical formulation. Numerical tests of this model with symmetrical formulation gave positive results in the case, where initial conditions and zero source term have been imposed. The case with a non-zero source is still under study.

3.2. *Polynomial basis*

As we discussed in the Introduction, one of the advantages of Trefftz-type methods is the flexibility in the choice of basis functions. The main condition is to satisfy the Trefftz property inside each element. To perform the numerical simulations, we have computed a polynomial basis, defined in the element of reference, using Taylor expansions of generating exponential functions - local solutions of the initial systems of equations. We have extended the algorithm for computing wave-polynomials for second order transient wave equation, proposed by Maciag in [22], to the first order ES and AS of dimension one and higher.

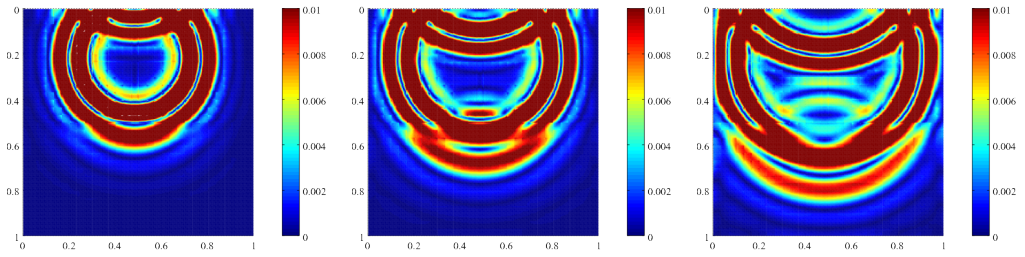

(a) $v(x, t = 0.567)$. (b) $v(x, t = 0.633)$. (c) $v(x, t = 0.700)$.

Figure 4. 2D EAS ($\alpha = \beta = 0.5$). Propagation of numerical velocity $v(x, t)$.

In 1D case it consists of couples of polynomial functions $(\hat{\phi}^v; \hat{\phi}^p)$ for velocity and pressure respectively, of degrees less or equal to $n\,(n = 0, 1, 2, 3)$, satisfying the Trefftz property, to provide n^{th} approximation order: $(0; -c_F)$, $(1; 0)$, $(x; -c_F^2\rho_F t)$, $(c_F t; -c_F\rho_F x)$, $(-\frac{x^2}{2} - \frac{c_F^2 t^2}{2}; c_F^2\rho_F xt)$, $(-c_F xt; c_F\rho_F(\frac{x^2}{2} + \frac{c_F^2 t^2}{2}))$, $(-\frac{x^3}{6} - \frac{xc_F^2 t^2}{2}; c_F\rho_F(\frac{c_F^3 t^3}{6} + \frac{x^2 c_F t}{2}))$, $(-\frac{c_F^3 t^3}{6} - \frac{x^2 c_F t}{2}; c_F\rho_F(\frac{x^3}{6} + \frac{xc_F^2 t^2}{2}))$. We refer the reader to see [42] for 2D AS and 2D ES extension.

3.3. *Numerical tests*

We present some numerical results obtained when applying the algorithm to the 2D elasto-acoustic problem (see more numerical tests in [42]).

It is worth noting that the currently developed code is a prototype MATLAB® version, which is, technically speaking, quite limited. This version has been created in order to explore the method and algorithm in general, and to perform some basic numerical tests for its validation. The development of a new high-performance software must be the next step. It will require the implementation of new propagators based on libraries, which have already been developed on the Carbon platform by Magique-3D and Total.

Wave propagation in coupled elasto-acoustic media is represented by the snapshots in the Figure 4.

The coupled fluid-solid medium is a unit square, and it contains two identical in form rectangular layers: acoustic on the top, and elastic at the bottom. The final time of propagation is $T = 1$. Medium parameters in acoustic media are $\rho_F = 1$, $c_F = 2$, in elastic media - $\rho_S = 1$, $\lambda = 1$, $\mu = 2$ (all parameters are nondimensionalized). We consider zero initial conditions, and introduce a source term in the middle of the acoustic layer. The source signal emitted at the source point src=(0.5,0.25) is represented by the first derivative of a Gaussian function, so that it takes approximately six elements per wavelength. Dirichlet conditions are imposed at the boundaries.

The numerics reproduce propagation characteristics that correspond perfectly to physical expectations. Even if the model is limited (large mesh of $30 \times 30 \times 30$ elements, Dirichlet boundaries, which causes many reflections), we can observe all type of waves (P, S - waves, incident, reflected waves and waves of P, S - head waves).

Figure 5 shows some results of convergence of the velocity in two-dimensional elastodynamic (a) and acoustic (b) cases.

The convergence curves have been computed for different approximation orders $(n = 0, 1, 2, 3)$, and they represent the numerical error as a function of cell size in logarithmic scale. The convergence in both cases is of order higher than the corresponding approximation order.

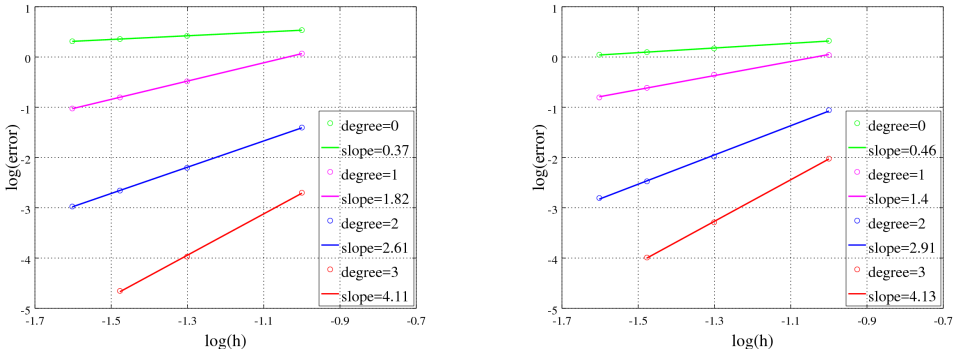

(a) 2D ES ($\alpha = \beta = 0.5$). (b) 2D AS ($\alpha = \beta = 0.5$).

Figure 5. Convergence of velocities v_S in elastodynamics and v_F in acoustics in function of cell size $h = \Delta x$.

4. Conclusion

We have applied the theory of Trefftz-DG method applied to the coupled Elasto-Acoustic System, we have studied the well-posedness of the problem, and proved error estimates in suitable mesh-dependent norms. The new space-time polynomial basis has been computed for numerical implementation of the method. We have developed a prototype code for 2D acoustic, elastodynamic, and elasto-acoustic problems, including the implementation of a source term, Dirichlet boundary conditions and rectangular mesh, which has been validated by the analytical solutions (see [42]). The convergence results are of higher order, compared to the classical DG methods. Moreover, Trefttz-DG variational formulation is simpler to compute, because it contains surface integration only, without any differential operators.

However, it is still early to discuss the performance of the code, before its optimization and paralleling. Thus, many directions are possible to explore, for both algorithmic and coding parts, such as: to continue studies of change-over between time layers in a case of implemented source [37], to study the optimal choice of penalty terms; to find the alternative to a global matrix inversion, which brings the main computational cost; to implement absorbing boundaries and perfectly matched layers for executing more proper simulations; to pass from simple rectangular meshes to more complicate (in space domain) forms - which is one of main advantages of Trefftz-DG methods. The last one gives the possibility of developing a hybrid method, based on numerical coupling of DG method in elastics, with Spectral Element Method (SEM) in acoustics, considering a Trefftz-DG transmission layer at the interface, in order to create software for a wider rane of applications.

The work, presented in this paper, is still under way. We have obtained very promising results, which deserve the development of a high-performance code, to be able to assess the method correctly.

Acknowledgements

This work is supported by the Inria - Total SA strategic action "Depth Imaging Partnership" (http://dip.inria.fr)

References

[1] R.M. Kirby, S.J. Sherwin, and B. Cockburn. *To CG or to HDG: A comparative study.* J of Sci Comp **51** (2012).

[2] I. Herrera. *Trefftz method: a general theory.* IIMAS Instituto de Investigaciones en Matematicas Aplicadas y en Sistemas (2000), 562–580.

[3] O.C. Zienkiewicz. *Trefftz type approximation and the generalized finite element method - history and developement.* Comp Ass Mech and Eng Sci **4** (1997), 305–316.

[4] J.S. Hesthaven, T. Warburton. *Nodal Discontinuous Galerkin methods. Algorithms, analysis, and applications.* Texts in Applied Mathematics **54** (2007), 1–370.

[5] A.C. Hidmarsh. *Solution of block-tridiagonal systems of linear algebraic equations.* Report UCID-30150, Lawrence Livermore Laboratory (1977).

[6] O. Cassenat, B. Després. *Application of an ultra-weak variational formulation of elliptic PDEs to the two-dimensional Helmholtz equation.* SIAM J Numer Anal **35** (1998), 255–299.

[7] E. Trefftz. *Ein Gegenstuck zum Ritzschen Verfahren.* Proc 2nd Int Cong Appl Mech Zurich (1926), 131–137.

[8] D.N. Arnold, F. Brezzi, B. Cockburn, and D. Marini. *Unified analysis of Discontinuous Galerkin methods for elliptic problems.* SIAM J Numer Anal **39(5)** (2002), 1749–1779.

[9] I. Babuska and M. Zlámal. *Nonconforming elements in the finite element method with penalty.* SIAM Journal on Numerical Analysis **10(5)** (1973), 863–875.

[10] F. Bassi, S. Rebay. *A high-order accurate discontinuous finite element method for the numerical solution of the compressible Navier-Stokes equations.* J Comp Phys **131** (1997), 267–279.

[11] F. Bassi, S. Rebay, G. Mariotti, S. Pedinotti, and M. Savini. *A high-order accurate discontinuous finite element method for inviscid and viscous turbomachinery flows.* Proceeding of 2nd European Conference on Turbomachinery, Fluid Dynamics and Thermodynamics, Antwerpen, Belgium (1997), 99–108.

[12] F. Brezzi, L.D. Marini. *Virtual element and Discontinuous Galerkin methods in recent developments in Discontinuous Galerkin finite element methods for partial differential equations.* Springer the IMA Volumes in Math and its Appl **157** (2014), 209–221.

[13] C.E. Baumann, J.T. Oden. *A discontinuous hp finite element method for convection-diffusion problems.* Comput Methods Appl Mech Eng **175** (1999), 311–341.

[14] P. Le Tallec. *Modélisation et calcul des milieux continus.* Les éditions de l'École Polytechnique (2008).

[15] J. Diaz. *Approches analytiques et numériques de problèmes de transmission et propagation d'ondes en régime transitoire. Application au couplage fluide-structure et aux méthodes de couches parfaitement adaptées.* Thèse de Doctorat de l'Université Paris VI (2005).

[16] E. Bossy. *Evaluation ultrasonore de l'os cortical par transimission axiale: modélisation et expérimentation in vitro et in vivo.* Thse de Doctorat de l'Université Paris VI (2003).

[17] H. Barucq, R. Djelloui, and E. Estecahandy, *Efficient DG-like formulation equipped with curved boundary edges for solving elasto-acoustic scattering problems.* International Journal for Numerical Methods in Engineering **98** (2014), 747–780.

[18] J. Jirousek. *Basis for development of large finite elements locally satisfying all fields equations.* Comp Meth Appl Mech Eng **14** (1978), 65–92.

[19] N. Leon, J. Jirousek. *A powerful finite element for plate bending.* Comp Meth Appl Mech Eng, **12** (1977), 77–96.

[20] T. Huttunen, P. Monk, and J.P. Kaipo. *Computational aspects of the ultra-weak variational formulation.* J Comput Phys **182** (2002), 27–46.

[21] K. Aki, P.G. Richards. *Quantitative seismology.* (2002).

[22] A. Maciag, J. Wauer. *Solution of the two-dimensional wave equation by using wave polynomials.* J Eng Math **51** (2006), 339–350

[23] S. Petersen, C. Farhat, and R. Tezaur. *A space-time Discontinuous Galerkin method for the solution of the wave equation in the time domain.* Internat J Numer Methods Engrg **79** (2009), 275–295.

[24] F. Kretzschmar, S.M. Schnepp, I. Tsukerman, and T. Weiland. *Discontinuous Galerkin methods with Trefftz approximation.* J Comp Appl Math **270** (2014), 211–222.

[25] D. Wang, R. Tezaur, and C. Farhat. *A hybrid discontinuous in space and time Galerkin method for wave propagation problems.* Int J Numer Methods Engrg **99** (2014), 263–289.

[26] H. Egger, F. Kretzschmar, S.M. Schnepp, and T. Weiland. *A space-time Discontinuous Galerkin Trefftz method for the time dependent Maxwell's equations.* SIAM J Sci Comput **37(5)** (2015), B689–B711.

[27] F. Kretzschmar, A. Moiola, and I. Perugia. *A priori error analysis of spacetime Trefftz discontinuous Galerkin methods for wave problems.* IMA Journal of Numerical Analysis, **36(4)** (2016), 1599–1635.

[28] L. Banjai, E. Georgoulis, and O. Lijoka. *A trefftz polynomial space-time discontinuous galerkin method for the second order wave equation.* SIAM Journal on Numerical Analysis **55(1)** (2017), 63–86.

[29] A. Moiola, I. Perugia. *A space-time Trefftz discontinous Galerkin method for the acoustic wave equation in first order formulation.* Numer Math DOI 10.1007/s00211-017-0910-x (2017).

[30] C. Farhat, I. Harari, and U. Hetmaniuk. *A Discontinuous Galerkin method with Lagrange multipliers for the solution of Helmholtz problems in the mid-frequency regime.* Comput Methods Appl Mech Eng **192** (2003), 1389–1419.

[31] R. Tezaur, C. Farhat. *Three-dimensional Discontinuous Galerkin elements with plane waves and Lagrange multipliers for the solution of mid-frequency Helmholtz problems.* Int J Numer Methods Eng **66** (2006), 796–815.

[32] G. Gabard. *Discontinuous Galerkin methods and plane waves for time-harmonic problems.* J Comput Phys **255** (2007), 1961–1984.

[33] R. Hiptmair, A. Moiola, and I. Perugia. *Plane wave Discontinuous Galerkin methods for the 2D Helmholtz equation: analysis of the p-version.* SIAM J Numer Anal **49** (2011), 264–284.

[34] A. Moiola, R. Hiptmair, and I. Perugia. *Plane wave approximation of homogeneous Helmholtz solutions.* Z Angew Math Phys **62(5)** (2011), 809–837.

[35] R. Hiptmair, A. Moiola, and I. Perugia. *Error Analysis of Trefftz-discontinuous Galerkin methods for the time-harmonic Maxwell equations.* Math Comp **82** (2013), 247–268.

[36] Z. Badics. *Trefftz-discontinuous Galerkin and finite element multi-solver technique for modeling time-harmonic EM problems with high-conductivity regions.* IEEE Transactions on Magnetics **50(2)** (2014), 401–404.

[37] P. Antonietti, I. Mazzierei. *A high-order Discontinuous Galerkin approximation to ordinary differential equations with applications to elastodynamics.* IMA J of Num Anal **162** (2016).

[38] C. Baldassari, H. Barucq, H. Calandra, B. Denel, and J. Diaz. *Performance analysis of a high-order Discontinuous Galerkin method application to the reverse time migration.* Communications in Computational Physics, **11(2)** (2012), 660–673.

[39] H. Barucq, J. Diaz, R. Djellouli, and E. Estecahandy. *High-order Discontinuous Galerkin approximations for elasto-acoustic scattering problems.* (2015)

[40] L.C. Wilcox, G. Stadler, C. Burstedde, and O. Ghattas. *A high-order discontinuous Galerkin method for wave propagation through coupled elasticacoustic media*,Comm in Comp Phys, Global Science Press, **229(24)** (2010), 9373–9396.

[41] J. Diaz. *Gar6more2D (Analytical Solutions of Wave Propagation Problems in Stratified Media)*, https://gforge.inria.fr/projects/gar6more2d/

[42] H. Barucq, H. Calandra, J.Diaz, and E. Shishenina. *Space-Time Trefftz - Discontinuous Galerkin Approximation for Elasto-Acoustics* Research Report Inria RR-9104 (hal-01614126), (2017).

[43] Misner CW. Efficient algorithms for layer assignment problems. In: Gottlob I, editor. Gravitation in a collapsing Universe. 2nd ed. San Francisco (CA): Freeman; 1973. p. 63–83. (Einstein's legacy; vol. 5).